Redox-Linked Structural Changes Associated with the Formation of a Catalytically Competent Form of the Diheme Cytochrome *c* Peroxidase from *Pseudomonas aeruginosa*[†,‡]

Aude Echalier,[§,||] Thomas Brittain,[⊥] Joshua Wright,[⊥] Svetlana Boycheva,[⊥] Gulnahar B. Mortuza,[#,▽] Vilmos Fülöp,[*,§] and Nicholas J. Watmough[*,#]

Department of Biological Sciences, University of Warwick, Coventry CV4 7AL, United Kingdom, School of Biological Sciences, University of Auckland, Auckland, New Zealand, and Centre for Metalloprotein Spectroscopy and Biology, School of Biological Sciences, University of East Anglia, Norfolk, NR4 7TJ, United Kingdom

Received October 15, 2007; Revised Manuscript Received November 29, 2007

ABSTRACT: A recombinant form of the prototypic diheme bacterial cytochrome *c* peroxidase (BCCP) from *Pseudomonas aeruginosa* (*Psa*CCP) has been expressed in *Escherichia coli* and purified to homogeneity. This material was used to carry out the first integrated biochemical, spectroscopic and structural investigation of the factors leading to reductive activation of this class of enzymes. A single, tightly bound, Ca^{2+} ion ($K = 3 \times 10^{10}$ M^{-1}) found at the domain interface of both the fully oxidized and mixed-valence forms of the enzyme is absolutely required for catalytic activity. Reduction of the electron-transferring (high-potential) heme in the presence of Ca^{2+} ions triggers substantial structural rearrangements around the active-site (low-potential) heme to allow substrate binding and catalysis. The enzyme also forms a mixed-valence state in the absence of Ca^{2+} ions, but a combination of electronic absorption, and EPR spectroscopies suggests that under these circumstances the low potential heme remains six-coordinate, unable to bind substrate and therefore catalytically inactive. Our observations strongly suggest that the two mixed-valence forms of native *Psa*CCP reported previously by Foote and colleagues (Foote, N., Peterson, J., Gadsby, P., Greenwood, C., and Thomson, A. (1985) *Biochem. J. 230*, 227−237) correspond to the Ca^{2+}-loaded and -depleted forms of the enzyme.

The bacterial cytochrome *c* peroxidases (BCCPs[1]) catalyze the two-electron reduction of hydrogen peroxide to water and link an essential detoxification pathway to respiration (*1*). Expression of BCCP is induced under microaerobic conditions in a range of bacteria including *Pseudomonas aeruginosa*, *Pseudomonas fluorecens*, *Pseudomonas nautica*, *Paracoccus pantotrophus* (formerly *Thiosphaera pantotropha* GB17), *Rhodobacter capsulatus*, *Methylococcus capsulatus*, *Neisseria gonorrheae* and *Nitrosomonas europaea* (*2*−*9*). In these organisms the electrons necessary for this reductive process are generally obtained from the cytochrome bc_1 complex of the bacterial electron transfer chain via either a reduced *c*-type cytochrome or a cupredoxin (*10*).

The enzymes so far characterized from these bacterial sources show some common features. All have been found to be dimeric with each subunit (35−40 kDa) comprising two domains with each domain containing a single covalently bound *c*-type heme (*3*, *11*−*13*). Within the fully oxidized forms the high-potential heme (HP heme) found in one domain has been shown to have His/Met axial ligation while the low potential heme (LP heme) in the other domain has His/His axial ligation or, in the case of the enzyme isolated from *N. europaea*, is five-coordinate with a proximal histidine ligand (*11*, *12*). Ca^{2+} ions have been found to be bound at the domain interface and have been implicated in functional roles in the enzymes from all species so far studied. In the oxidized form the single Ca^{2+} ion shows unusual hepta-coordination, with three ligands provided by peptide backbone and amide carbonyl oxygen atoms (*11*). The remaining four ligands are provided by coordinated water molecules, two of which further hydrogen bonded to the carboxylic acid terminal of the propionate side chains of the HP heme, although these later two water molecules were not observed in the case of the *R. capsulatus* enzyme

[†] This work was funded by the UK BBSRC (Award B10987 to N.J.W. and V.F.) and the Wellcome Trust (Award 066363/Z/01/Z to N.J.W. and T.B.). A.E. was in receipt of a UK EPSRC studentship.

[‡] The coordinates of the structure reported in this manuscript have been deposited with the PDB accession code 2vhd.

* Authors to whom correspondence should be addressed. N.J.W.: School of Biological Sciences, University of East Anglia, Norwich, NR4 7TJ, United Kingdom; tel, +44 (1603) 592179; fax, +44 (1603) 592250; e-mail, n.watmough@uea.ac.uk. V.F.: Department of Biological Sciences, University of Warwick, Coventry CV4 7AL, United Kingdom; tel, +44 (0)24 7657 2628; fax, +44 (0)24 7652 3701; e-mail, vilmos@globin.bio.warwick.ac.uk.

[§] University of Warwick.

[||] Present address: Laboratory of Molecular Biophysics, University of Oxford, Oxford OX1 3QU, United Kingdom.

[⊥] University of Auckland.

[#] University of East Anglia.

[▽] Present address: Division of Protein Structure, MRC National Institute for Medical Research, The Ridgeway, Mill Hill, London NW7 1AA, United Kingdom.

[1] Abbreviations: APX, ascorbate peroxidase; BCCP, bacterial cytochrome *c* peroxidase; CT-band, charge-transfer band; EDTA, ethylenediamine tetraacetic acid; HP heme, high-potential heme; LP heme, low-potential heme; *Pap*CCP; *Paracoccus pantotrophus* CCP; *Psa*CCP, *Pseudomanas aeruginosa* CCP

10.1021/bi702064f CCC: $40.75
Published on Web 01/25/2008

(*14*). A number of previous studies have investigated the mode of action of these enzymes and have established that with the exception of the enzyme purified from *N. europaea* (*12*) the as isolated enzymes are fully oxidized and catalytically incompetent (*15*−*17*). These can be activated by partial reduction to yield a mixed-valence form in which the electron-transferring (HP) heme is ferrous and the peroxidatic LP heme becomes five-coordinate ferric. Reaction of the mixed-valence form of the enzyme with hydrogen peroxide in the presence of reductant initially leads to the formation of an Fe(IV)−oxo species known as "compound I"[2] which is then reduced to a form of the enzyme in which both hemes are oxidized state, but unlike the enzyme as isolated is functionally active within the catalytic cycle (*18*).

Despite these similarities the CCPs obtained from various bacterial species show some significant differences. For example the BCCP from *P. pantotrophus* (*Pap*CCP) has hemes with reduction potentials of +226 mV and −150mV, and was originally reported to bind two Ca^{2+} ions in the oxidized state. The high-affinity site was reported to bind Ca^{2+} with a K_d of 1.2 μM, a value which shifts to 3 μM on reduction of the HP heme of the enzyme, while occupancy of low-affinity site (K_d = 520 μM in the oxidized form of the enzyme) was considered to be important for dimerization (*13*, *19*). However recent structural investigations have identified only a single binding site (*20*). In contrast the CCP purified from *Pseudomonas stutzeri* is reported as having a single interdomain Ca^{2+} binding site with an equilibrium constant in the nM range for the mixed-valence form of the protein (*21*). The *N. europaea* enzyme exhibits redox potentials of +470 mV and −260 mV and the crystal structure of the catalytically competent oxidized state indicates that the single Ca^{2+} binding site is fully occupied.

Potentially important differences have also been reported in the structural changes associated with the formation of the mixed-valence form for the BCCPs isolated from *P. nautica* (*22*) and *P. pantotrophus* (*20*), which are most likely to be related to the choice of crystallization conditions. X-ray diffraction and biochemical studies of the fully oxidized form of the native (e.g., non-recombinant) enzyme from *P. aeruginosa* showed it to have a single Ca^{2+} binding site (*11*) and possess hemes with redox potentials of +320 mV (HP heme) and −330 mV (LP heme). Previous investigations of the *Psa*CCP have established the general reaction mechanism for this enzyme including the need for reduction of the HP heme in order to produce a catalytically active mixed-valence form of the enzyme although the structure of this form has not previously been reported. Moreover there have been no biochemical studies on the role of Ca^{2+} ions in the activation of *Psa*CCP.

We describe the expression and purification of recombinant *Psa*CCP expressed in *Escherichia coli* which we used to obtain the X-ray structure of the mixed-valence form. The structure of the mixed-valence *Psa*CCP, reported here for the first time, reveals the extensive changes around the active site heme and which take place in response to reduction of the high-potential heme that prepare the enzyme for catalysis. Recombinant *Psa*CCP was also used to investigate the characteristics of the Ca^{2+} binding site and its impact on the catalytic activity of the enzyme. This work shows that interconversion of the spectroscopically distinct "active" and "inactive" mixed-valence forms of the enzyme depends on the occupancy of this Ca^{2+} binding site rather than irreversible proteolytic inactivation as had previously been proposed (*23*). The outcome of this integrated biochemical, spectroscopic and structural study of the factors leading to reductive activation of the BCCPs is an experimentally testable model for the activation of the enzyme from *P. aeruginosa* and the role of the mixed-valence form of the enzyme in turnover.

MATERIALS AND METHODS

Recombinant *Psa*CCP was expressed in *E. coli* JM109 (DE3) co-transformed with pETCCP and pEC86 plasmids. pETCCP was constructed by amplifying the *P. aeruginosa* ccp gene (*24*) using the following primers: NM1.fwd (GCGG*CCATGG*GGTCCTCGCAACTG) and NM3.rev (CCGCGTCCCGCGGAATAAT*AAGCTT*CCC). The amplified product was digested with *Nco*I and *Hin*dIII and cloned into the expression vector pET21d (Novagen) to yield pETCCP. Note that incorporating a *Nco*I site into the NM1.fwd causes the glutamine residue at position 2 of the amino acid sequence to be substituted by a glycine. Since the first 22 amino acids of *Psa*CCP comprise a cleavable leader sequence that directs the apoenzyme to the periplasmic space via the sec-pathway, this substitution has no effect on the mature enzyme. The plasmid pEC86 is a pCYCA derived plasmid containing the *E. coli* ccm operon which increases the levels of those proteins required for covalent attachment of *c*-type hemes into periplasmic proteins and their subsequent maturation to the fully formed holoenzymes (*25*). The cytochrome c_{551} which was used as an electron donor in the enzymic activity assay was expressed in *E. coli* using a plasmid which was a kind gift from Prof. F. Cutruzzolà (Rome, Italy) (*26*).

Transformed cells were grown in 750 mL of Terrific Broth (TB) supplemented with 50 μg mL^{-1} ampicillin and 34 μg mL^{-1} chlorampenicol at 28 °C with shaking at 160 rpm for 48 h and without IPTG induction. Cells were harvested by centrifugation and the *Psa*CCP initially released from the periplasm by treatment with polymixin (*27*). The enzyme was further purified by ammonium sulfate fractionation (30−55%) followed by sequential chromatography on S-Sepharose and Superdex-75, following extensive dialysis. The purity of the final enzyme preparation was verified by SDS−PAGE and UV/vis spectroscopy. Typically the ratio of the absorbance at 407 and 280 nm (A_{407}:A_{280}) was >4.2, which is similar to the value reported for the native protein (*28*). Purification of recombinant *Psa*CCP expressed in *E. coli* co-transformed with pETCCP and pEC86, as outlined above, allowed the preparation of up to 8 mg of pure enzyme per liter of cell culture.

For structural studies a form of the enzyme containing a C-terminal $(His)_6$ tag was used. This required a modified expression vector (pETCCP-Histag) which was constructed by amplifying the region of pET-CCP between the T7 promoter and the 3′ end of the *Psa ccp* gene using pET-

[2] The nomenclature that has been used to describe intermediates in the catalytic cycle of *Psa*CCP is confusing. Although the active site heme is an Fe(IV)−oxo species, neither the porphyrin macrocycle or an amino acid has been oxidized to provide the extra electron required for scission of the O−O bond as is observed in Compound I of Horseradish Peroxidase (HRP) and Yeast CCP respectively. Therefore strictly speaking the initial product of the reaction of *Psa*CCP with H_2O_2 should be referred to as Compound II.

CCP as a template. The following primers were used both to amplify the fragment of interest and to insert appropriate restriction sites: **T7 Promoter** TAA TAC GAC TCA CTA TAG GG **CCP1** TTT CGC *CTC GAG* TTC CGC GGG ACG CGC CGT GGT. The PCR product was digested with *Xba*I and *Xho*I and cloned into the expression vector pET-26b vector (Novagen) to yield pETCCP-Histag. For expression of recombinant his-tagged *Psa*CCP *E. coli* JM109(DE3) was co-transformed with pETCCP-Histag and pEC86. Transformed cells were grown in 800 mL of TB supplemented with chloramphenicol and kanamycin for 24−28 h at 30 °C.

His-tagged *Psa*CCP was purified from cell paste derived from 3 L of cell culture as follows. The cell paste was resuspended in 30 mL of 50 mM Hepes, 200 mM NaCl, 4 mM $CaCl_2$, 60 mM imidazole, 0.01% Triton X-100, pH 7.5 and the suspension was supplemented with 0.1 mg/mL lysozyme and protease inhibitors (2 mM AEBSF, 2 μM leupeptin, 2 μM pepstatin) prior to sonication (1 min per liter of culture). Cell debris was separated from the soluble fraction by centrifugation at 21,000 rpm for 60 min (4 °C) and the supernatant loaded on a Ni-sepharose column. The column was initially washed with 60 mM imidazole, followed by a second wash with 88 mM imidazole. His-tagged *Psa*CCP was eluted with 140 mM imidazole and at this stage the A_{407}:A_{280} is approximately 3.7. Fractions containing enzyme were pooled and the buffer exchanged for 50 mM MES, 4 mM $CaCl_2$, pH 6.0 and loaded on a prepacked Resource Q (1 mL). The protein was eluted with a salt gradient from 0 to 1 M NaCl. Samples containing enzyme were again pooled and ammonium sulfate added to a final concentration of 4 M before loading on a prepacked Resource Phe (1 mL). The protein elutes toward the end of the decreasing ammonium sulfate gradient with an A_{407}:A_{280} ratio that is greater than 5.0.

Mass spectrometry was performed using an Agilent 1100 series XCT Ion Trap MS and a Voyager De Pro MALDITOF MS. UV/visible absorption spectroscopy was performed using a Shimadzu UV-2501 PC instrument.

In experiments involving the investigation of the role of Ca^{2+} ions in the structure and function of *Psa*CCP all solutions were prepared using "Ca^{2+} free" water (USF Elga Maxima ultrapure water) and all samples were stored and handled without contact with glassware. Samples of *Psa*CCP were buffer exchanged as necessary by passage through a small (10 cm × 1 cm) Sephadex column equilibrated with the appropriate buffer. Catalytic activity using cytochrome c_{551} was determined according to the procedures previously described by (*28*).

Mixed-valence *Psa*CCP was prepared by adding sodium ascorbate to a final concentration of 10 mM. The formation of the mixed-valence form of the enzyme was monitored by absorption spectroscopy in the 390 nm to 450 nm region. Ca^{2+} was removed from the mixed-valence form of the enzyme (20 μM *Psa*CCP) by addition of EDTA to a final concentration of 2 mM, and the reaction was monitored by observing the optical density change at 390 nm over a period of 60 min. Samples of *Psa*CCP devoid of Ca^{2+} were prepared by passing the EDTA-treated mixed-valence *Psa*CCP sample down a small Sephadex column equilibrated with the appropriate buffer. Fluorescence, circular dichroism and stopped flow experiments were performed on an Applied Photophysics Π*180.

CD spectra were deconvoluted into the various secondary structural components using publicly available software (K2D).

EPR spectra were recorded using an ER-200D X-band spectrometer (Spectrospin, Bruker), equipped with a liquid helium flow cryostat (ESR-9, Oxford Instruments), and interfaced to an ESP1600 computer. Spectra at 9.41 GHz were collected using 2.0 mW microwave power with a modulation amplitude of 2 mT.

Crystallization, X-ray Data Collection, Structure Determination and Refinement. After extensive screening, crystals of mixed-valence *Psa*CCP were obtained from 24% PEG 600, 0.2 M imidazole malate pH 5.5, 20 mM DTT. All the components used for the crystallization experiments were purged with oxygen-free nitrogen for 20 min and the crystallization trays (Nextal) used to set up the crystallization experiments were fitted with an airtight seal. After opening a crystallization tray the crystallization drop was quickly coated with a thin layer of mineral oil to prevent oxidation and crystals were directly flash-frozen in a nitrogen stream. Initial X-ray diffraction experiments were performed at the SRS, Daresbury (U.K.), but the final data set was collected at 100 K at EMBL, Hamburg (Germany) using synchrotron radiation. Data were processed using the HKL suite of programs (*29*). The remaining structure factor calculations were performed using programs supported by CCP4 (*30*).

Molecular replacement (*31*) was performed using the dimer coordinates of the mixed-valence from of the *P. denitrificans* enzyme ((*20*), PDB code: 2C1V). Refinement of the structure was carried out by alternate cycles of REFMAC (*32*) using noncrystallographic symmetry (NCS) restrains and manual rebuilding in O (*33*). Water molecules were added to the atomic model automatically by Arp/wARP (*34*), and at the last steps of refinement all the NCS restrains were released. The final model includes all 323 residues, the two covalent heme groups and the bound Ca^{2+} for both subunits of the dimer. Data collection and refinement statistics are given in Table 1.

RESULTS

Spectroscopic Properties of the Mixed-Valence Form of PsaCCP. The UV/vis absorption spectrum of oxidized recombinant *Psa*CCP in the region 350−700 nm closely matches that previously published for the native enzyme. The addition of sodium ascorbate to the oxidized enzyme in the presence of Ca^{2+} ions rapidly leads to formation of the mixed-valence species as indicated by changes in all regions of the spectrum (Figure 1). The Soret region broadens, leading to perceived loss of intensity, and its peak shifts to 421 nm. This is due to the spectrum of the ferrous HP heme with a maximum at 420 nm overlaying the spectrum of the high-spin ferric LP heme which appears as a broad shoulder between 390 and 405 nm. There is an increase in intensity in the α/β region of the spectrum with new peaks at 521 and 557 nm that are consistent with the reduction of one low-spin heme. In the 600−700 nm region of the spectrum there is a significant increase in the intensity of the weak feature at ~640 nm. Broad weak bands in this region of the spectrum are associated with the ligand−metal charge-transfer (CT-band) of the sixth ligand of high spin ferric hemes with a proximal histidine ligand (*35*).

Table 1: Crystallographic Data Collection and Refinement Statistics[a]

	mixed-valence form
Data Collection	
synchrotron, detector and wavelength (Å)	EMBL X11 MAR CCD 165 mm; 0.8115
space group	*C*2
unit cell (*a*, *b*, *c* (Å), β (deg))	173.2, 44.8, 106.2, 106.7
resolution (Å)	(76−2.30)
observations	167124
unique reflections	34786
$I/\sigma(I)$	16.0 (1.6)
R_{sym}[b]	0.089 (0.717)
completeness (%)	98.6 (95.8)
V_M/solvent content (%)	2.8/56
molecules per AU	2
Refinement	
all non-hydrogen atoms	5407
water molecules	289
R_{cryst}[c]	0.184 (0.246)
reflections used	32981 (2351)
R_{free}[d]	0.246 (0.333)
reflections used	1805 (132)
R_{cryst} (all data)[c]	0.187
mean temperature factor (Å^2)	42.9
rmsds from ideal values	
bonds (Å)	0.016
angles (deg)	1.6
DPI coordinate error (Å)	0.30

[a] Numbers in parentheses refer to values in the highest resolution shell. [b] $R_{sym} = \sum_j\sum_h|I_{h,j} - \langle I_h\rangle|/\sum_j\sum_h\langle I_h\rangle$ where $I_{h,j}$ is the *j*th observation of reflection *h*, and $\langle I_h\rangle$ is the mean intensity of that reflection. [c] $R_{cryst} = \sum||F_{obs}| - |F_{calc}||/\sum|F_{obs}|$ where F_{obs} and F_{calc} are the observed and calculated structure factor amplitudes, respectively. [d] R_{free} is equivalent to R_{cryst} for a randomly selected subset of reflections not used in the refinement.

When the mixed-valence form of *Psa*CCP was treated with an excess of EDTA, the spectrum showed a number of significant changes. Over the course of approximately 40 min the Soret region of the spectrum narrowed with a progressive loss of absorbance at 380 nm (Figure 1). In addition the removal of Ca^{2+} ions from the mixed-valence form of the enzyme leads to an almost complete abolition of the CT-band at ~640 nm (Figure 1 inset). These spectral changes are consistent with the ferric LP heme undergoing a transition from a high-spin state to a low-spin state.

In the presence of 0.5 mM $CaCl_2$ the X-band EPR spectrum of the oxidized recombinant *Psa*CCP is complex with resonances at $g = 3.41$, 3.00, and, 2.27 (Figure 2; upper trace). The form of the spectrum is identical to that reported for the native enzyme (*23*, *36*). The signals at $g = 3.41$ and $g = 3.00$ represent the g_z components of two low-spin ferric hemes; the His/Met coordinated HP heme and the His/His coordinated LP heme.

On treatment with ascorbate to form the mixed-valence state the EPR spectrum changes (Figure 2; lower trace). There is the expected loss of the $g = 3.41$ signal that is associated with reduction of the HP heme, and the $g = 3.00$, $g = 2.27$ species is replaced by a very sharply defined rhombic trio ($g_z = 2.86$, $g_y = 2.39$, $g_x = 1.53$). In a sense this is surprising because these signals must arise from a low-spin (e.g., six coordinate) ferric heme, yet the loss of the distal histidine residue (His^{71}) from the LP heme would be expected to yield a high-spin ferric species (as seen in the room-temperature UV/vis absorbance spectrum) that is able to bind substrate. However, the observation of a single low-spin ferric heme at cryogenic temperatures is entirely consistent with work on native *Psa*CCP (*23*, *36*) and the CCPs isolated from *P. pantotrophus* (*37*) and *P. stutzeri* (*21*). Moreover the presence of this species in the EPR spectrum is always associated with the presence of a ~640 nm CT-band in the room-temperature absorbance spectrum.

Formation of the mixed-valence form of recombinant *Psa*CCP in the presence of EDTA is also characterized by the loss of the $g = 3.41$ species (Figure 2; middle trace). In this case the LP heme gives rise to a rhombic trio that is similar in form and intensity to the oxidized and suggests that in the absence of Ca^{2+} ions the ligand set to the LP heme remains low-spin ferric with His/His axial ligand set. This is consistent with the room-temperature optical spectrum which suggests there is no high-spin ferric heme present under these conditions.

Removal of Ca^{2+} Ions from the Mixed-Valence Species. Quantitative analysis of this process indicated a single-exponential time course for the optical density change as a function of time with an associated rate constant of 8×10^{-4} s^{-1} ($\pm 2 \times 10^{-4}$ s^{-1}) over the pH range 6.0− 9.0. The rate of loss of Ca^{2+} from the enzyme was found to be essentially independent of pH. However, the extent of removal of Ca^{2+} by EDTA was sensitive to the pH at which the measurements were made, being much less at acid pH. (We can rule out the possibility that the diminished absorbance change at 380 nm seen at low pH arises from a pH dependence of the absorption spectrum of the mixed-valence state or Ca^{2+} depleted enzyme as the spectrum of the Ca^{2+} depleted enzyme produced at pH 9.0 and then lowered to pH 6.0 is unaltered by the change in pH.) Using the known pH dependence of the Ca^{2+} binding constant of EDTA (*29*, *30*) it was possible to determine the effective binding constant for Ca^{2+} to the mixed-valence form of the *Psa*CCP using the extent of the 380 nm change as a function of pH. The data was best fitted to a binding constant of 3×10^{10} M^{-1} (Figure 3). Simultaneous monitoring of the peroxidase activity and the electronic absorption spectrum of the enzyme during treatment with EDTA showed that the loss of catalytic function followed a decrease in optical density at 380 nm (Figure 4).

When Ca^{2+} depleted *Psa*CCP was rapidly mixed with Ca^{2+} in the range 1−100 mM, the time course of the optical density change in the Soret region of the spectrum showed the presence of two kinetic phases. These two kinetic phases showed somewhat different difference spectra (Figure 5A). At a wavelength of 380 nm the time course of the reaction was sigmoidal while at 405 nm (a wavelength isosbestic in the overall spectral change) two reactions associated with optical density changes of different sign could be observed with associated rates of 0.003 s^{-1} and 0.03 s^{-1} (Figure 5B). At other wavelengths the sum of two simple exponential processes could be seen. The observed rates and amplitudes of the two kinetic phases were found to be independent of $[Ca^{2+}]$.

Structural Changes upon Activation. Circular dichroism studies of the secondary structural changes in the protein associated with the mixed-valence formation and the subsequent removal of Ca^{2+} ions indicated a conversion of β structure to random coil on mixed-valence formation and a

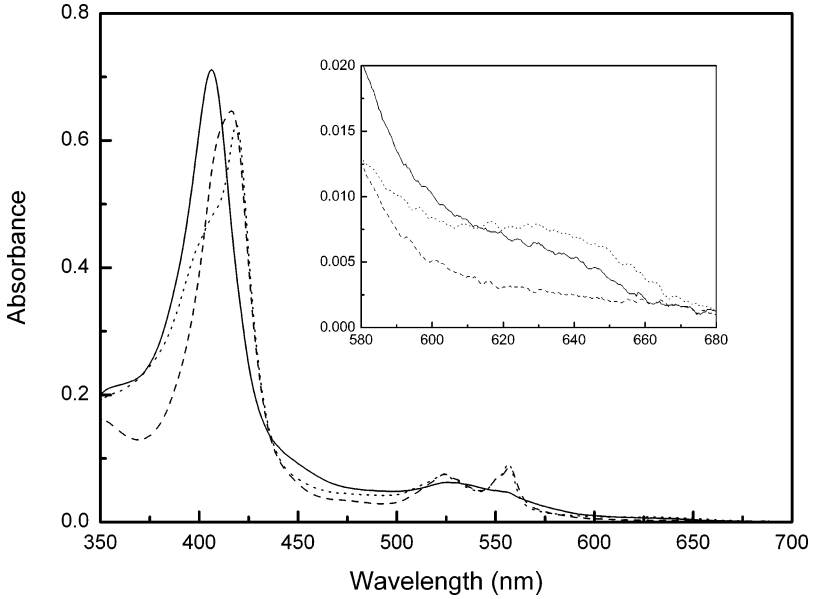

FIGURE 1: Spectral changes associated with the removal of Ca^{2+} from mixed-valence *Psa*CCP. Oxidized recombinant *Psa*CCP (3 μM) was dissolved in 5 mM Mes/5 mM Hepes pH 6.5 (solid line). The mixed-valence state of CCP was obtained by the addition of 10 mM ascorbate (dotted trace) in the presence of 0.5 mM $CaCl_2$. Ca^{2+} ions were subsequently removed from the mixed-valence enzyme by the addition of 10 mM EDTA followed by 45 min incubation at room-temperature (dashed trace). The inset shows the detail of the near infrared region of the spectrum.

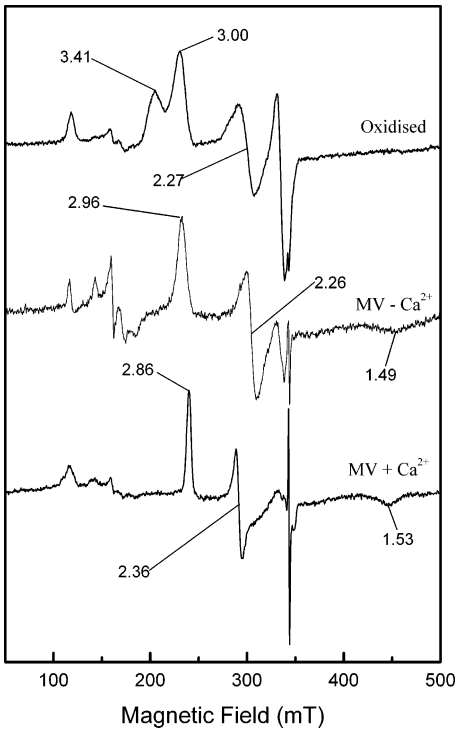

FIGURE 2: The effect of Ca^{2+} on the X-band EPR spectra of the mixed-valence form of *Psa*CCP. Oxidized recombinant *Psa*CCP (~40 μM) was dissolved in 5 mM Mes/5 mM Hepes pH 6.5 and the spectrum recorded at 10 K. The mixed-valence state of *Psa*CCP was obtained by the addition of 10 mM ascorbate and the spectrum rerecorded in the presence or absence of Ca^{2+} ions. Microwave frequency = 9.41 GHz, microwave power =2 mW and modulation amplitude = 10 G.

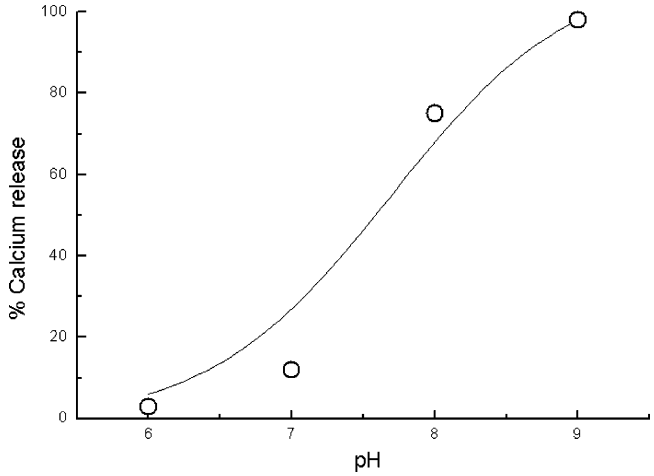

FIGURE 3: Determination of the Ca^{2+} binding constant for the mixed-valence form of *Psa*CCP. The experimentally determined extent of Ca^{2+} release as a function of pH (○), measured from the decrease in absorbance at 380 nm, is shown compared to the calculated release (—) based on literature values for the pH dependence of the equilibrium constant for EDTA−Ca^{2+} binding using a cytochrome *c* peroxidase−Ca^{2+} binding equilibrium constant of 3×10^{10} M.

conversion of α to β structure on subsequent removal of Ca^{2+}. Parallel investigations monitored via fluorescence spectroscopy showed that the addition of EDTA to the mixed-valence form of the enzyme led to an increase in the intensity of the emission spectrum in the 340−345 nm region, on a time scale identical to that observed for the loss of absorption intensity reported above.

Both oxidized (PDB entry 1eb7 (*11*)) and mixed-valence forms (PDB entry 2vhd) of the enzyme have very similar three-dimensional structures (Figure 6); superimposition of 267 common Cα atoms gives 1.03 Å root-mean-square (rms) deviation. Comparison of the two redox forms identifies four regions (residues 68−76, 91−115, 215−243 and 277−283) with different conformation. These residues account for 22% of the polypeptide chain and are located near the two heme groups. Generally, the structural rearrangement is very similar to that found in *Pap*CCP (*20*) showing that the overall structures of the corresponding redox states are more similar to each other than structures with different redox forms of

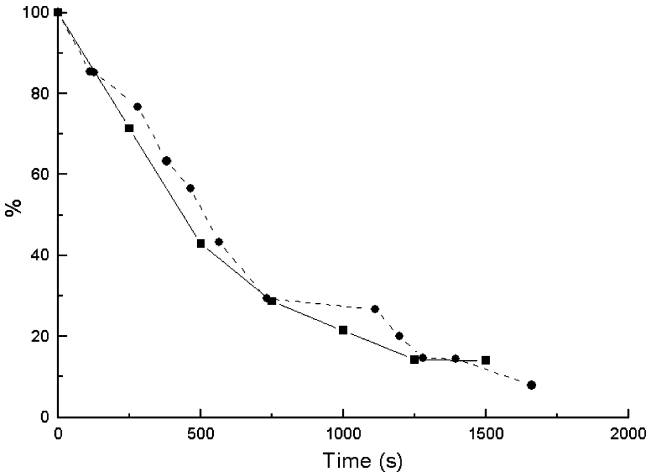

FIGURE 4: Correlation of Ca^{2+} removal and loss of catalytic activity in the mixed-valence form of *Psa*CCP. The time course for Ca^{2+} removal from *Psa*CCP at pH 9.0 in 100 mM borate buffer (■) is compared with the enzymic activity of the enzyme (●). The scale on the *Y*-axis (%) represents the percentage of the original activity and bound calcium in the absence of added EDTA.

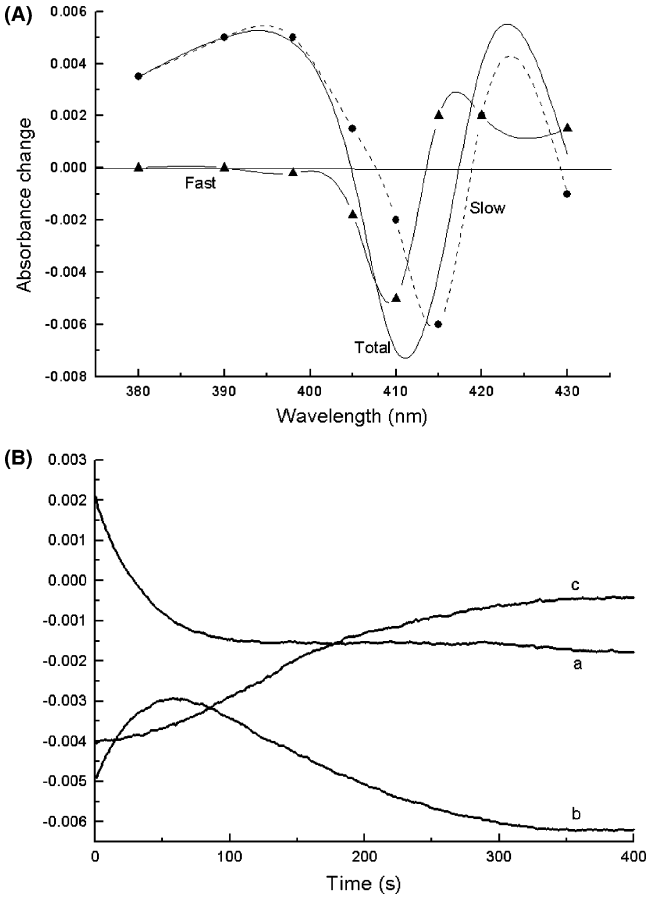

FIGURE 5: Kinetic difference spectra for reaction of the mixed-valence form of *Psa*CCP with Ca^{2+} ions. Panel A shows the contribution of the fast (▲) and slow (●) kinetic phases of Ca^{2+} binding to calcium depleted *Psa*CCP together with the overall spectral change (—) associated with the Ca^{2+} binding process. Panel B shows the time courses for the reaction of 25 mM Ca^{2+} with 2 μM calcium-depleted *Psa*CCP at pH 7.0 in 10 mM phosphate buffer at (a) 420 nm, (b) 405 nm and (c) 380 nm. The traces are offset for clarity.

the protein originating from the same organism (0.95 Å rms for 297 and 0.59 Å rms for 320 common Cα atoms in the oxidized mixed-valence forms, respectively).

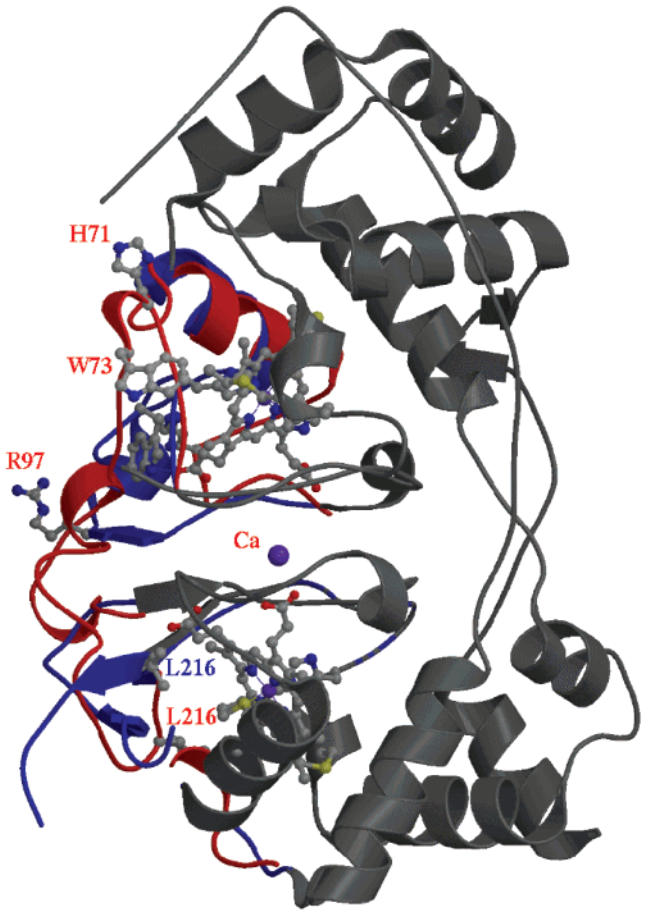

FIGURE 6: Redox-linked changes in the structure of *Psa*CCP. Structural differences (residues 68−76, 91−115, 215−243 and 277−283) are colored blue and red for the oxidized and mixed-valence forms of the enzyme respectively. The hemes, the calcium ion and some key residues of the structures are in ball-and-stick representation. Figures were drawn with MolScript (*46*, *47*) and rendered with Raster3D (*48*).

Conformational Changes at the HP (Electron Receiving) Heme Site. The coordination of the HP heme by His^{201} and Met^{275} remains unaltered in the two redox states. Following one-electron transfer from electron donors to the HP heme, the orientation of its D propionate group changes, leading to a loss of a hydrogen bond to the main chain Leu216 amide (Figure 7A). This suggests that the reduction of the heme group might be coupled to proton uptake by its propionate group, in a process known as a redox-coupled Bohr effect (*38*), which in turn initiates a cascade of structural changes that prepares the enzyme for turnover. A similar trigger for structural rearrangement has been reported for the *P. pantotrophus* enzyme (*20*).

The spatial arrangement of the residues between the two heme groups does not significantly change upon activation. The co-ordination sphere of the Ca^{2+} binding site between the two heme domains is also identical in both oxidation states and contains no charged ligand in the first coordination shell. The seven ligands are the amide oxygen of Asn79, the main-chain carbonyls of Thr256 and Pro258 and four water molecules (Figure 7A). The nearest carboxylate group is the A propionate of the HP heme, which is linked to the calcium via two water molecules.

Conformational Changes at the LP (Peroxidatic) Heme Site. The simultaneous reduction and proton uptake of the

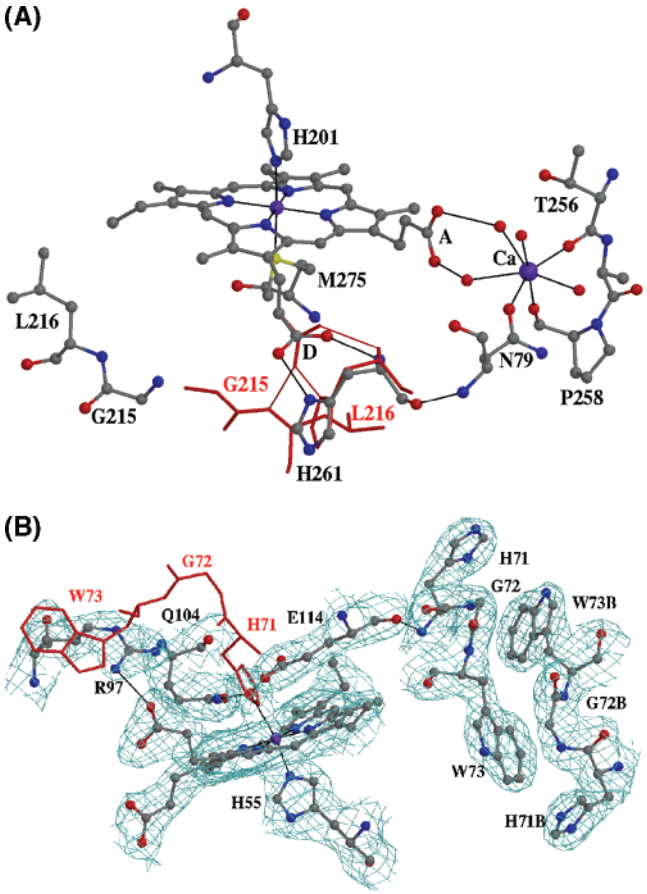

FIGURE 7: The heme and Ca^{2+} binding sites of *Psa*CCP. Panel A: The HP heme of the mixed-valence form of *Psa*CCP. The propionate D group of the heme undergoes a conformational change upon reduction and loses the interaction with the main chain amide of Leu216. The corresponding conformation in the oxidized form is shown in red. The propionate A group is linked to the Ca^{2+} ion via two water molecules and does not change under activation. Panel B: The LP heme and dimer interface of the mixed-valence form of *Psa*CCP. The loop carrying His71 moves away to the interface of the homodimer. This structure is stabilized by π-stacking interaction between the aromatic side chain of Trp73 and the peptide bond of Gly72 of the opposite chain (labeled as G72B). The peroxide binding site is occupied by a water molecule, which is hydrogen bonded to Gln104 and Glu114. The corresponding residues in the oxidized form are shown in red. The SIGMAA (*47*) weighted $2mF_o - \Delta F_c$ electron density using phases from the final model of the half-reduced form is contoured at the 1.0σ level, where σ represents the rms electron density for the unit cell. Contours more than 1.5 Å from any of the displayed atoms have been removed for clarity. Thin lines indicate hydrogen bonds.

HP heme triggers a cascade of structural changes around the LP heme. Residue Arg97 moves significantly to initiate further structural changes. This residue switches from the domain interface to form a hydrogen bond to one of the propionates of the LP heme (Figure 7B). Although the proximal coordination of His55 stays unaltered, residues at the distal side of the heme change dramatically. The loop carrying His71 moves away to the interface of the homodimer. This structure is stabilized by π-stacking interaction between the aromatic side chain of Trp73 and the peptide bond of Gly72 of the opposite chain. The movement of this loop makes the peroxidatic site accessible for substrates and also introduces two other conserved residues Gln104 and Glu114. These two residues lie within hydrogen bonding distance of the heme iron bound water (Figure 7B) and have been suggested to play critical roles in the formation and stabilization of the oxyferryl intermediate of both the *N. europaea* and *P. pantotrophus* CCPs.

DISCUSSION

Our studies of the mixed-valence form of *Psa*CCP in solution indicate that Ca^{2+} binds to at a single binding site with an affinity of approximately 3×10^{10} M^{-1}. The binding of a single Ca^{2+} ion is clearly a prerequisite for steady-state catalytic activity, and only in the presence of saturating concentrations of Ca^{2+} ions does the mixed-valence state contains a high-spin heme center that can bind substrate. These data are consistent with existing models of activation for this class of enzymes in which reduction of the HP heme leads to a cascade of conformational changes which includes the LP heme losing its distal histidine ligand so that it can bind substrate.

This paper represents the first report of the dependence of the activity of *Psa*CCP upon Ca^{2+} ions. This is perhaps not surprising as not only is there is a clear relationship between catalytic activity and the presence of Ca^{2+} ions in a number of other BCCPs including the enzymes from *P. denitrificans*, *P. nautica* and *P. stutzeri* (*2*, *19*, *21*), but in addition the structure of the oxidized (*11*) and mixed-valence (Figure 6) *P. aeruginosa* enzyme clearly shows a Ca^{2+} ion bound at the domain interface. The relationship between Ca^{2+} ions and catalytic activity in the *Psa*CCP was almost certainly clouded by two issues.

First of all CCP isolated from *P. aeruginosa* (native *Psa*CCP) is very susceptible to proteolytic cleavage by elastase which is expressed by the organism under the same growth conditions that yield high levels of CCP (*39*, *40*). Second it was established by Foote and colleagues that native *Psa*CCP could be isolated in both catalytically "active" and "inactive" forms which were spectroscopically distinct (*23*). Although these authors argued that inactivity was correlated with the extent of proteolysis, they did not provide any data to support this assertion (this issue is discussed in more detail elsewhere (*1*)).

It is however very important to remember that Foote et al. (*23*) completed their study on the native *Psa*CCP before the role for Ca^{2+} ions in activation of diheme CCPs was suggested by Pettigrew (*19*). As a consequence it is very helpful to compare the spectroscopic data we present here for the mixed-valence forms ($\pm Ca^{2+}$ ions) of the recombinant *Psa*CCP, which is expressed in *E. coli* and not susceptible to proteolysis, with the extensive spectroscopic data that is available for the mixed-valence forms of the "active" and "inactive" types of native *Psa*CCP (*18*, *23*, *36*). This information is summarized in Table 2 and strongly suggests that the "active" and "inactive" forms of the native *Psa*CCP in fact represent Ca^{2+}-loaded and -depleted forms. The key diagnostic features of the Ca^{2+}-loaded and catalytically active mixed-valence form are the presence of a ligand−metal charge-transfer band at ~640 nm in the room-temperature UV/vis absorbance spectrum (Figure 1 inset) and a very sharp rhombic trio of resonances ($g_z = 2.86$, $g_y = 2.39$, $g_x = 1.53$) in the 10 K X-band EPR spectrum (Figure 2). A similar correlation between these spectroscopic features, Ca^{2+}-loading and catalytic activity has been demonstrated in the CCPs isolated from *P. pantotrophus* and *P. stutzeri* (*21*, *37*).

Table 2: Spectroscopic Characteristics of Different Forms of the Mixed-Valence (Half-Reduced) State of *P. aeruginosa* CCP from Native and Recombinant Sources

	native *Psa*CCP		recombinant *Psa*CCP	
	"active"	"inactive"	Ca^{2+} bound	Ca^{2+} depleted
UV/vis absorbance (maxima)				
Soret (both hemes)	420 nm (∼395 nm)	421 nm (∼410 nm)	421 nm (∼395 nm)	421 nm
visible (both hemes)	557 nm 525 nm	557 nm 525 nm	557 nm 525 nm	557 nm 525 nm
near IR (LP Fe(III) heme)	∼630 nm	absent	∼640 nm	absent
X-band EPR (10 K) (LP Fe(III) heme)	$g_z = 2.85$ $g_y = 2.26$ $g_x = \sim 1.54$	$g_z = 3.00$ $g_y = 2.26$ $g_x = \sim 1.4$	$g_z = 2.86$ $g_y = 2.36$ $g_x = 1.53$	$g_z = 2.96$ $g_y = 2.26$ $g_x = 1.49$

Circular dichroism measurements show that the mixed-valence form of *Psa*CCP in the presence of Ca^{2+} form has a lower β-sheet content than the oxidized form. Structural studies revealed that only two β-strands (211−213 and 244−246) are common between the two forms; the others involving residues 95−97, 214−218 and 233−237 form random coil and a short helix (233−236) upon reduction (Figure 6). The structural rearrangement of strand 95−97 has a particular consequence, it breaks the main-chain hydrogen bonding pattern between the two domains and presumably makes the molecule more flexible for domain movements. Consequently the structurally more rigid oxidized form does not release Ca^{2+}, since the continuous formation of β-strands between the two domains makes the interface inaccessible to EDTA. In contrast the Ca^{2+} is exchangeable in the mixed-valence form thanks to conformational changes initiated by reduction of the HP heme site. The presence of two different, concentration independent, rates of calcium binding is consistent with a structurally heterogeneous population in the calcium depleted enzyme in which conformational alterations rate limit the calcium rebinding process.

Thus both functional and structural studies support a model in which the Ca^{2+}-binding site of the *P. aeruginosa* enzyme must be fully occupied for activation to occur through reduction of the HP heme. A similar model for the mechanism of activation has been proposed for the enzyme purified from *P. pantotrophus* (*20*) which is also isolated in a resting fully oxidized conformation. The cascade of structural changes around the LP heme of the *P. aeruginosa* enzyme that is initiated by reduction of the HP heme appears to be mediated by the movement of Arg97. This movement is triggered by a redox-linked protonation of the HP heme D propionate group, something that might be expected to require the reduction of the HP heme iron to produce a change in the electron density on the D propionate group. Such changes have been observed in other systems (*41*). The HP heme however possesses two propionate groups of which only one appears to undergo a redox-linked Bohr effect. A plausible explanation for this finding which also explains the significant role played by the bound Ca^{2+} ion relates to the unusual co-ordination chemistry of the Ca^{2+} binding site. Most Ca^{2+} binding sites contain at least one carboxylate and often more; for example the distal Ca^{2+} binding site of Horseradish Peroxidase C uses three carboxylate ligands (*42*). We suggest that the bound Ca^{2+} serves to modulate the pK_a of the HP heme A propionate that serves as its ligand such that it is effectively never protonated. This arrangement would imply that the only site on the HP heme that can accommodate a proton when the heme iron becomes reduced is the carboxyl group on the second, D, propionate and that this event is responsible for initiating the structural changes.

As well as initiating structural reorganization of the distal pocket to remove the blocking axial histidine (His71) reduction of the HP heme also orientates Gln104 and Glu114 to allow them to participate in catalysis (Figure 7B). This leads to the question as to whether these changes are sufficient to activate the enzyme or if other structural changes are required to endow catalytic competence? In this respect it is interesting that the structures of the mixed-valence, and thus catalytically active, forms of *Psa*CCP and *Pap*CCP clearly have Arg97 (Arg111 in the *Pap*CCP structure) interacting with the D-propionate of the LP heme. A similar arrangement is also found in the catalytically active oxidized form of the *N. europaea* CCP (*12*) and in the OUT form of the mixed-valence CCP from *Pseudomonas nautica* (*22*) so it is useful to consider the consequences of this changed electrostatic environment.

A combined DFT and QM/MM study of the active site heme in cytochrome $P450_{cam}$ suggests that the interaction of positively charged residues with the heme propionates has a role in stabilizing the porphyrin π-cation radical associated with the Fe(IV)−oxo intermediate responsible for substrate hydroxylation (*43*). This proposed role for electrostatic shielding of heme propionates has been tested experimentally in a variant form of ascorbate peroxidase (APX) known as APX3M that has been engineered to stabilize the radical generated in APX compound I on a tryptophan residue rather than on the heme porphyrin macrocycle (*44*). Substitution of an arginine residue (Arg172) that interacts with one of the heme propionates with asparagine in this APX3M background further inhibits the enzyme's ability to form a porphyrin π-cation radical (*44*).

As well as providing new insights into the structural basis of reductive activation of this class of bacterial enzymes, the work presented here provides an important link between the extensive historical literature on native *Psa*CCP and our emerging understanding of the role of Ca^{2+} ions in enzyme activation. Our demonstration of the true nature of the active and inactive forms of *Psa*CCP will allow re-evaluation of the extensive set of variable temperature magnetic CD data collected by those workers. Moreover the ability to mutagenize individual residues in a diheme BCCP for which there are high-resolution structures of both the oxidized and mixed-valence forms will illuminate the roles of individual residues in the catalytic cycle and allow us to address a number of outstanding questions regarding both the reductive activation and turnover of this class of enzymes, in particular, whether the Ca^{2+}-loaded mixed-valence form of the enzyme forms part of the catalytic cycle of *Psa*CCP (*15*), or if this state is only required for the first turnover of the enzyme which then follows the reaction mechanism that has recently been proposed, on the basis of protein film voltammetry studies, for the *N. europaea* enzyme (*45*).

ACKNOWLEDGMENT

We are grateful for access to the facilities of SRS, Daresbury, U.K., and the European Molecular Biology Laboratory beam line X11 at the DORIS storage ring of Deutsches Elektronen-Synchrotron, Hamburg, Germany. Finally we would like to thank Professor Colin Greenwood (University of East Anglia) for introducing T.B., V.F. and N.J.W. to this fascinating enzyme. During the final preparation of this manuscript Colin passed away after a long illness. This contribution is dedicated to his memory.

REFERENCES

1. Fülöp, V., Watmough, N. J., and Ferguson, S. J. (2001) Structure and Enzymology of Two Bacterial Diheme Enzymes: Cytochrome cd_1 Nitrite Reductase and Cytochrome *c* Peroxidase, *Adv. Inorg. Chem. 51*, 163−204.
2. Alves, T., Besson, S., Duarte, L. C., Pettigrew, G. W., Girio, F. M., Devreese, B., Vandenberghe, I., Van Beeumen, J., Fauque, G., and Moura, I. (1999) A cytochrome *c* peroxidase from *Pseudomonas nautica* 617 active at high ionic strength: expression, purification and characterization, *Biochim. Biophys. Acta 1434*, 248−259.
3. Arciero, D. M., and Hooper, A. B. (1994) A di-heme cytochrome *c* peroxidase from *Nitrosomona europea* catalytically active in both the oxidized and half-reduced states, *J. Biol. Chem. 269*, 11878−11886.
4. Ellfolk, N., and Soininen, R. (1970) *Pseudomonas* cytochrome c peroxidase. I. Purification procedure, *Acta Chemica Scand. [B] 24*, 2126−2136.
5. Goodhew, C., Wilson, I., Hunter, D., and Pettigrew, G. (1990) The cellular location and specificity of bacterial cytochrome *c* peroxidases, *Biochem. J. 271*, 707−712.
6. Hu, W., De Smet, L., Van Driessche, G., Bartsch, R. G., Meyer, T. E., Cusanovich, M. A., and Van Beeumen, J. (1998) Characterization of cytochrome c_{556} from the purple phototrophic bacterium *Rhodobacter capsulatus* as a cytochrome *c* peroxidase, *Eur. J. Biochem. 258*, 29−36.
7. Pettigrew, G. (1991) The cytochrome *c* peroxidase of *Paracoccus denitrificans*, *Biochim. Biophys. Acta 1058*, 25−27.
8. Zahn, J. A., Arciero, D. M., Hooper, A. B., Coats, J. R., and DiSpirito, A. A. (1997) Cytochrome *c* peroxidase from *Methylococcus capsulatus* Bath, *Arch. Microbiol. 168*, 362−372.
9. Turner, S., Reid, E., Smith, H., and Cole, J. (2003) A novel cytochrome *c* peroxidase from *Neisseria gonorrhoeae*: a lipoprotein from a Gram-negative bacterium, *Biochem. J. 373*, 865−873.
10. Pettigrew, G. W., Echalier, A., and Pauleta, S. R. (2006) Structure and mechanism in the bacterial dihaem cytochrome *c* peroxidases, *J. Inorg. Biochem. 100*, 551−567.
11. Fülöp, V., Ridout, C., Greenwood, C., and Hajdu, J. (1995) Crystal structure of the di-haem cytochrome *c* peroxidase from *Pseudomonas aeruginosa*, *Structure 3*, 1225−1233.
12. Shimizu, H., Schuller, D. J., Lanzilotta, W. N., Sundaramoorthy, M., Arciero, D. M., Hooper, A. B., and Poulos, T. L. (2001) Crystal structure of *Nitrosomonas europaea* cytochrome *c* peroxidase and the structural basis for ligand switching in bacterial di-heme peroxidases, *Biochemistry 40*, 13483−13490.
13. Gilmour, R., Goodhew, C., Pettigrew, G., Prazeres, S., Moura, I., and Moura, J. (1993) Spectroscopic characterization of cytochrome *c* peroxidase from *Paracoccus denitrificans*, *Biochem. J. 294*, 745−752.
14. De Smet, L., Savvides, S. N., Van Horen, E., Pettigrew, G., and Van Beeumen, J. J. (2006) Structural and mutagenesis studies on the cytochrome *c* peroxidase from *Rhodobacter capsulatus* provide new insights into structure-function relationships of bacterial di-heme peroxidases, *J. Biol. Chem. 281*, 4371−4379.
15. Foote, N., Turner, R., Brittain, T., and Greenwood, C. (1992) A quantitative model for the mechanism of action of the cytochrome *c* peroxidase of *Pseudomonas aeruginosa*, *Biochem. J. 283*, 839−843.
16. Brittain, T., and Greenwood, C. (1992) Complex formation between the copper protein azurin and the cytochrome *c* peroxidase of *Pseudomonas aeruginosa*, *J. Inorg. Biochem. 48*, 71−77.
17. Gilmour, R., Goodhew, C., Pettigrew, G., Prazeres, S., Moura, J., and Moura, I. (1994) The kinetics of the oxidation of cytochrome *c* by *Paracoccus* cytochrome *c* peroxidase, *Biochem. J. 300*, 907−914.
18. Greenwood, C., Foote, N., Gadsby, P. M. A., and Thomson, A. J. (1988) A di-haem cytochrome *c* peroxidase (*Pseudomonas aeruginosa*): its activation and catalytic cycle, *Chem. Scr. 28A*, 79−84.
19. Gilmour, R., Prazeres, S., McGinnity, D., Goodhew, C., Moura, J., Moura, I., and Pettigrew, G. (1995) The affinity and specificity of Ca^{2+}-binding sites of cytochrome *c* peroxidase from *Paracoccus denitrificans*, *Eur. J. Biochem. 234*, 878−886.
20. Echalier, A., Goodhew, C. F., Pettigrew, G. W., and Fülöp, V. (2006) Activation and catalysis of the di-heme cytochrome *c* peroxidase from *paracoccus pantotrophus*, *Structure 14*, 107−117.
21. Timóteo, C. G., Tavares, P., Goodhew, C. F., Duarte, L. C., Jumel, K., Girio, F. M., Harding, S., Pettigrew, G. W., and Moura, I. (2003) Ca^{2+} and the bacterial peroxidases: the cytochrome *c* peroxidase from *Pseudomonas stutzeri*, *J. Biol. Inorg. Chem. 8*, 29−37.
22. Dias, J. M., Alves, T., Bonifacio, C., Pereira, A. S., Trincao, J., Bourgeois, D., Moura, I., and Romao, M. J. (2004) Structural basis for the mechanism of Ca^{2+} activation of the di-heme cytochrome *c* peroxidase from *Pseudomonas nautica* 617, *Structure 12*, 961−973.
23. Foote, N., Peterson, J., Gadsby, P., Greenwood, C., and Thomson, A. (1985) Redox-linked spin-state changes in the di-haem cytochrome c_{551} peroxidase from *Pseudomonas aeruginosa*, *Biochem. J. 230*, 227−237.
24. Ridout, C. J., James, R., and Greenwood, C. (1995) Nucleotide sequence encoding the di-haem cytochrome c_{551} peroxidase from *Pseudomonas aeruginosa*, *FEBS Lett. 365*, 152−154.
25. Reincke, B., Thöny-Meyer, L., Dannehl, C., Odenwald, A., Aidim, M., Witt, H., Ruterjans, H., and Ludwig, B. (1999) Heterologous expression of soluble fragments of cytochrome c_{552} acting as electron donor to the *Paracoccus denitrificans* cytochrome *c* oxidase, *Biochim. Biophys. Acta 1411*, 114−120.
26. Russell, B. S., Zhong, L., Bigotti, M. G., Cutrozzolà, F., and Bren, K. L. (2003) Backbone dynamics and hydrogen exchange of *Pseudomonas aeruginosa* ferricytochrome c_{551}, *J. Biol. Inorg. Chem. 8*, 156−166.
27. Gordon, E. H. J., Steensma, E., and Ferguson, S. J. (2001) The cytochrome *c* domain of dimeric cytochrome cd_1 of *Paracoccus pantotrophus* can be produced at high levels as a monomeric holoprotein using an Improved *c*-type cytochrome expression system in *Escherichia coli*, *Biochem. Biophys. Res. Commun. 281*, 788.
28. Foote, N., Thompson, A., Barber, D., and Greenwood, C. (1983) *Pseudomonas* cytochrome c_{551} peroxidase. A purification procedure and study of CO-binding kinetics, *Biochem. J. 209*, 701−707.
29. Otwinowski, Z., and Minor, W. (1997) Processing of X-ray Diffreaction dat Collected in Oscillation Mode, *Methods Enzymol. 276*, 307−326.
30. Collaborative Computational Project Number 4 (1994) The CCP4 suite: programs for protein crystallography, *Acta Crystallogr., Sect. D 50*, 760−763.
31. Navaza, J. (2001) Implementation of molecular replacement in AMoRe, *Acta Crystallogr., Sect. D: Biol. Crystallogr. 57*, 1367−1372.
32. Murshudov, G. N., Vagin, A. A., Lebedev, A., Wilson, K. S., and Dodson, E. J. (1999) Efficient anisotropic refinement of macromolecular structures using FFT, *Acta Crystallogr., Sect. D 55*, 247−255.
33. Jones, T. A., Zou, J. Y., Cowan, S. W., and Kjeldgaard, M. (1991) Improved methods for building protein models in electron density maps and the location of errors in these models, *Acta Crystallogr.*, Sect. A. *47*, 110−119.
34. Perrakis, A., Morris, R., and Lamzin, V. S. (1999) Automated protein model building combined with iterative structure refinement, *Nat. Struct. Biol. 6*, 458−63.
35. Watmough, N. J., Cheesman, M. R., Butler, C. S., Little, R. H., Greenwood, C., and Thomson, A. J. (1998) The dinuclear center of cytochrome bo_3 from *Escherichia coli*, *J. Bioenerg. Biomembr. 30*, 55−62.
36. Aasa, R., Ellfolk, N., Rönnberg, M., and Vänngård, T. (1981) Electron paramagnetic resonance studies of *Pseudomonas* cytochrome *c* peroxidase, *Biochim. Biophys. Acta 670*, 170−175.

37. Prazeres, S., Moura, J., Moura, I., Gilmour, R., Goodhew, C., Pettigrew, G., Ravi, N., and Huynh, B. (1995) Mössbauer characterization of *Paracoccus denitrificans* cytochrome *c* peroxidase. Further evidence for redox and calcium binding-induced heme-heme interaction, *J. Biol. Chem. 270*, 24264−24269.
38. Papa, S., Guerrieri, F., and Izzo, G. (1979) Redox Bohr-effects in the cytochrome system of mitochondria, *FEBS Lett. 105*, 213−216.
39. Ellfolk, N., Rönnberg, M., and Osterlund, K. (1991) Structural and functional features of *Pseudomonas* cytochrome *c* peroxidase, *Biochim. Biophys. Acta 1080*, 68−77.
40. Soininen, R., and Ellfolk, N. (1975) *Pseudomonas* cytochrome *c* peroxidase. X. The effect of *Pseudomonas* neutral proteinase on the enzyme molecule, *Acta Chem. Scand. [B] 29*, 134−136.
41. Bento, I., Teixeira, V. H., Baptista, A. M., Soares, C. M., Matias, P. M., and Carrondo, M. A. (2003) Redox-Bohr and other cooperativity effects in the nine-heme cytochrome *c* from *Desulfovibrio desulfuricans* ATCC 27774: crystallographic and modeling studies, *J. Biol. Chem. 278*, 36455−36469.
42. Gajhede, M., Schuller, D., Henriksen, A., Smith, A., and Poulos, T. (1997) Crystal structure of horseradish peroxidase C at 2.15 Å resolution, *Nat. Struct. Biol. 4*, 1032−1038.
43. Guallar, V., Baik, M. H., Lippard, S. J., and Friesner, R. A. (2003) Peripheral heme substituents control the hydrogen-atom abstraction chemistry in cytochromes P_{450}, *Proc. Natl. Acad. Sci. U.S.A. 100*, 6998−7002.
44. Barrows, T. P., and Poulos, T. L. (2005) Role of electrostatics and salt bridges in stabilizing the compound I radical in ascorbate peroxidase, *Biochemistry 44*, 14062−14068.
45. Bradley, A. L., Chobot, S. E., Arciero, D. M., Hooper, A. B., and Elliott, S. J. (2004) A distinctive electrocatalytic response from the cytochrome *c* peroxidase of *Nitrosomonas europaea*, *J. Biol. Chem. 279*, 13297−13300.
46. Kraulis, P. J. (1992) Molscript—A program to produce both detailed and schematic plots of protein structures, *J. Appl. Crystallogr. 24*, 946−950.
47. Esnouf, R. M. (1997) An extensively modified version of MolScript that includes greatly enhanced coloring capabilities, *J. Mol. Graphics Modell. 15*, 112−113, 132−134.
48. Merritt, E. A., and Murphy, M. E. (1994) Raster3D Version 2.0. A program for photorealistic molecular graphics, *Acta Crystallogr., Sect. D 50*, 869−873.

BI702064F